Feasibility study of macroscopic simulations of nanodosimetric parameters for proton therapy

Vasi, Fabiano ; Schmidli, Kevin ; Hälg, Roger A ; Schneider, Uwe

Abstract: In view of the potential of treatment plan optimization based on nanodosimetric quantities, fast Monte Carlo methods for obtaining nanodosimetric quantities in macroscopic volumes are important. In this work, a "fast" method for obtaining nanodosimetric parameters from a clinical proton pencil beam in a macroscopic volume is compared with a slow and detailed method. Furthermore, the variations of these parameters, when obtained with the Monte Carlo codes TOPAS and NOREC, are investigated.

DOI: https://doi.org/10.1002/mp.14178

Feasibility Study of Macroscopic Simulations of Nanodosimetric Parameters for Proton Therapy

Fabiano Vasi[1,2], Kevin Schmidli[2], Roger A. Hälg[1,2], Uwe Schneider[1,2]
[1]Radiotherapy Hirslanden, Witellikerstrasse 40, 8032 Zurich, Switzerland
[2]Department of Physics, University of Zurich, Winterthurerstrasse 190, 8032 Zurich, Switzerland

Version typeset April 6, 2020

Fabiano Vasi. email: fabiano.vasi2@uzh.com

Abstract

Purpose: In view of the potential of treatment plan optimization based on nanodosimetric quantities, fast Monte Carlo methods for obtaining nanodosimetric quantities in macroscopic volumes are important. In this work, a "fast" method for obtaining nanodosimetric parameters from a clinical proton pencil beam in a macroscopic volume is compared with a slow and detailed method. Furthermore, the variations of these parameters, when obtained with the Monte Carlo codes TOPAS and NOREC, are investigated.

Methods: Monte Carlo track structure simulations of 1 keV - 100 MeV protons and 12 eV - 1 MeV electrons in a volume of 8 nm^3 liquid water provided us with an atlas of cluster size distributions. Two kinds of ionization cluster size distributions were recorded, counting all ionizations or only ionizations directly produced by the primary particle.

The simulations of the proton pencil beam were performed in two different ways. A "fast" method where only the protons were simulated and a "slow and detailed" method where protons and electrons were simulated in order to obtain spectra at different depths. The obtained spectra were then convoluted with cluster size distributions.

Results: It was shown that the nanodosimetric quantity F_2 from the "fast" method is, depending on the location, between 43.6% and 63.6% smaller than the F_2 obtained by the "slow and detailed" method. However, it was also shown that variations of nanodosimetric quantities are even larger when the cluster size distributions of the electrons are simulated with the Monte Carlo code NOREC, i.e. the cumulative F_2 probabilities obtained with NOREC were between 50.8% and 75.5% smaller than the F_2 probabilities obtained with TOPAS.

Conclusions: As long as the uncertainties of different Monte Carlo codes are not improved, it is feasible to only simulate protons in a macroscopic volume. It must be noted however, that the uncertainty is in the order of 100 %.

Contents

I. Introduction

The use of ionizing radiation to treat cancer has a long history. Many types of radiations have been used to achieve the best possible tumor control. It has been found that the quantity absorbed dose is not adequate to describe the biological effectiveness of ionizing radiation. The absorbed dose required to produce a given biological effect depends among others on radiation quality, which is defined by the type and energy of particles forming a radiation field. Therefore, the assessment of the absorbed dose alone is not sufficient to determine the biological effectiveness of ionizing radiation in radiotherapy. To remedy this deficiency the concept of the relative biological effectiveness (RBE) was introduced. RBE of a given radiation is defined as the ratio of the reference dose (usually high energetic photons) to the dose of the test radiation which produces the same defined biological damage.

In order to understand the different biological impacts of different radiation qualities as well as to study the stochastic nature of radiation interactions, microdosimetry was founded over a half century ago. In microdosimetry it is assumed that microscopic fluctuations of energy depositions are important because the response of each cell will depend on the energy deposition within the cell. In addition, variations within the dimensions of the cell are considered of importance since radiation sensitive targets are on the subcellular level (e.g. cell nucleus). Microdosimetry can especially be of value at low doses (e.g. a few mGy), where most cells do not receive any energy deposition.[1] In case the subcellular structure of dosimetric interest is a short segment of DNA, it is called nanodosimetry.[2]

Nanodosimetry embarks on a new, more fundamental strategy than classical dosimetry. The goal of nanodosimetry is to find a physical measurand, which is related to the track structure and characterizes the biological damage better than the concept of absorbed dose. In nanodosimetry, usually ionization cluster size distributions (ICSD), i.e. number of ionizations produced by a particle and/or its secondaries in a specified volume, are measured or simulated.[3,4,5,6,7] In the following this specified volume is called the basic interaction volume (BIV).

One of the most critical biological damages induced by radiation in the cell is the DNA double-strand break, where the DNA is completely separated into at least two parts. A DNA double-strand break is usually defined as two single-strand breaks within 10 base-pairs

on opposite strands.[5 8 9 10] Moreover, it has been shown that double-strand breaks correlate well with at least two to five ionizations in spheres with diameters of 1 - 4 nm.[11] Therefore, important quantities in nanodosimetry are the cumulative cluster size probabilities. The cumulative probability F_2 describes the probability of a particle track to cause a cluster size of two or greater in a basic interaction volume. The size of the basic interaction volume is often chosen such that it corresponds to a volume of 10 base-pairs. It is then assumed that the cumulative probability F_2 in such a volume is proportional to DNA double-strand breaks.[4]

It is currently not possible to perform track structure simulations of realistic treatment plans (volume size $\sim 10^{-2}\,\mathrm{m}^3$) in a reasonable time. In a study carried out by Casiraghi et al.[12] the feasibility of carbon-ion and proton plan optimization based on nanodosimetric quantities in a simplified geometry of five macroscopic voxels was investigated. The authors showed that nanodosimetric quantities can be uniformly distributed in an array of five target voxels while simultaneous sparing the adjacent voxels. The reported calculation times for their treatment plans was in the order of days and weeks for protons and carbon ions respectively.

Another approach proposed by Alexander et al.[13] was to record conditional ionization cluster size distributions of protons in cylinders with a diameter of 2.3 nm and a height of 3.4 nm. Conditional cluster size distributions give the relative probability to obtain a cluster size since they disregard the cluster size zero. The cylinders were superimposed on the proton track structure in a water cube with a length of 1 µm. The resulting conditional mean ionization cluster size $M_1^{C_1}$ and the cumulative probabilities $F_2^{C_1}$ and $F_3^{C_1}$ to obtain a cluster size equal or larger than two or three ionizations,respectively, were acquired. The energy dependence of these quantities was subsequently fitted with power laws of several parameters.

Ramos-Méndez et al.[14] recently provided a database of cluster size distributions for protons and ions scored in 1800 small cylinders (with a length of 3.4 nm and a diameter of 2.3 nm) which were embedded in a large cylinder (with a length of 161 nm and a diameter of 30.4 nm) mimicking DNA chromatin fiber. Moreover, a database of the mean cluster size M_1, the conditional mean cluster size $M_1^{C_2}$, the cumulative probability for two or more ionizations F_2, and the conditional cumulative probability $F_3^{C_2}$ was provided for 0.5 - 100 MeV u^{-1} protons, 1 - 100 MeV u^{-1} alphas, and 1 - 1000 MeV u^{-1} lithium ions, beryllium ions, boron ions, carbon ions, nitrogen ions, and oxygen ions.

I.. INTRODUCTION

In addition, Ramos-Méndez and colleagues implemented a fast calculation method to score nanodosimetric quantities in treatment planning of proton and ion therapy.[14] In their approach they utilize the previously calculated database. They simulate proton pencil beams and a carbon spread-out Bragg peak in a cubic water phantom. Particle type and energy are scored in millimetric sized voxels, the corresponding nanodosimetric quantity is looked-up in their database, and is then weighted with either track length or deposited energy. They conclude that the deposited energy weighted method approaches the result of full track structure simulations. An open question of the method of Ramos-Méndez et al. is, if the simulation of only primary particle tracks is accurate enough in a macroscopic volume. Their pre-calculated cluster size distributions do not take into account electrons from adjacent primary proton tracks, since electrons are not included in the scored spectra, which could lead to potential uncertainties.

In clinical practice, it is important to have short computation times to obtain nanodosimetric parameters in macroscopic volumes, which represent a part of the patient volume. In this work, we investigated the feasibility of macroscopic simulations for nanodosimetric quantities. For this purpose, we examined two different methods to calculate nanodosimetric probabilities from a clinical proton pencil beam at different depths.

First an atlas of independent cluster size distributions for protons and electrons was acquired. Two types of cluster size distributions were included in the atlas. In the first kind, called "primaries and secondaries", all created ionizations were considered. For the second type, which was called "only primaries", only the ionizations produced by the primary particles were counted. In a second step, the spectra of all charged particles from a clinical proton pencil beam at different depths of a macroscopic volume were acquired by detailed Monte Carlo simulations.

The obtained particle spectra were then utilized in two ways: In the so-called "slow and detailed" method, the particle spectra of all particles were convoluted with the corresponding "only primaries" cluster size distributions. In the second method, which we call the "fast" method, the primary proton spectra at different depths were convoluted with the corresponding primaries and secondaries cluster size distributions. Hence, in the "fast" method the contributions of the secondary electrons are only included in the pre-simulated cluster size distributions.

To find out if the "fast" method, in which only primary particles are simulated in the

macroscopic volume, are accurate enough for the calculation of nanodosimetric quantities for threatment planning system, it was compared to the time consuming "slow and detailed" method.

II. Methods

II.A. Nanodosimetric Simulations of Cluster Size Distributions

A database of treatment plan independent cluster size distributions has to be simulated only once. Cluster size distributions depend on particle type, energy, the size of the volume and the material. The cluster size distributions were simulated inside a sphere of water with a volume of 8 nm^3 (diameter = 2.48 nm). A single sphere was used for the calculations of the atlas of cluster size distributions. We call such a sphere in which the ionzations are scored the basic interaction volume (BIV). Water is used as a substitute for tissue. For the Monte Carlo simulations of the cluster size distributions the GEANT4-DNA extension (Geant4 version 10.02 patch 01) was used.[15 16 17] The default physics constructor was used for liquid water. Cluster size distributions were simulated for protons and electrons. For each particle type, the validity of the underlying physical model has to be considered. The energy ranges chosen were as large as possible and inside the validity range of the underlying model class. The primary energies to simulate ionization cluster size distributions for protons and electrons were 1 keV - 100 MeV and 12 eV - 1 MeV, respectively. A reasonable number of energy bins were chosen such that intervals, where the ionization cluster size distribution changes strongly, are covered well. For each radiation energy 10^5 or 10^6 histories were simulated, such that the relative error on the cluster size distribution is small compared to the errors of the simulation codes.

Two kinds of ionization cluster size distribution were investigated. The first method to determine cluster size distributions (termed "only primaries") considered only ionizations caused by the primary particle itself. For the determination of these "only primaries" ionization cluster size distributions, the water sphere with a volume of 8 nm^3 was surrounded by vacuum. The implemented beam source was a monoenergetic point-source and it was positioned at the surface of the water sphere so that the emitted particles initial direction was perpendicular to the surface of the sphere. This type of cluster size distribution is needed

for the implementation of the "slow and detailed" method as is explained in section II.C..
The second kind of ionization cluster size distributions (termed "primaries and secondaries") considers ionizations from primary and secondary particles. For the determination of these ionization cluster size distributions, the spherical basic interaction volume of $8\,\mathrm{nm}^3$ was placed in the middle of a water cube with an edge length of 400 nm. The monoenergetic point-source was positioned on the surface of the spherical basic interaction volume and the initial direction of the emitted particles was perpendicular to that surface. Since the basic interaction volume is surrounded by water, it is possible for secondary particles, which left the sphere, to scatter back inside and possibly produce additional ionizations in the basic interaction volume. This type of ionization cluster size distribution is needed for the "fast" method which is defined in section II.C..
Moreover, two different Monte Carlo codes were used to simulate ionization cluster size distributions from electrons. The reason for this is that simulations of electrons have the highest uncertainties, especially for low-energy electrons ($< 100\,\mathrm{eV}$), due to differences in interaction cross-sections and models used[18 19 20 21]. The two different Monte Carlo codes used for the simulations of the electrons were GEANT4-DNA and NOREC[22]. NOREC was specifically designed to simulate electron tracks in liquid water. From ionization cluster size distributions P_ν typical nanodosimetric quantities can be determined such as the mean ionization cluster size $M_1 = \sum_{\nu=1}^{\infty} P_\nu \cdot \nu$ or the cumulative probability $F_2 = \sum_{\nu=2}^{\infty} P_\nu$, where ν is the number of ionizations.

II.B. Particle Spectra Produced by a Clinical Pencil Beam

To obtain nanodosimetric parameters in a patient sized volume, a proton pencil beam was simulated in a water tank with dimensions of $10\,\mathrm{cm} \times 10\,\mathrm{cm} \times 35\,\mathrm{cm}$ in $x \times y \times z$ direction, respectively. The phase space of the Gantry 2 at the Paul Scherrer Institute (PSI) was used to simulate the proton pencil beam. A large number of 2.5×10^7 protons with a nominal energy of 99.65 MeV were simulated (50 statistically independent samples with 5×10^5 histories each). An initial nominal beam energy spread of 0.7 % existed. Proton position and momentum direction of the source were sampled with a bivariate 2D Gaussian corresponding to an area of $1\,\mathrm{cm}^2$.

The protons were simulated in a water tank with TOPAS 3.0.p1 (Geant4 version 10.02

patch 01). The distance from the beam source perpendicular to the water tank surface was 47.8 cm.

The goal was to record the particle spectra at different depths. For this reason, 26 spherical scoring volumes with diameters of 600 µm were placed along the central axis z of the water tank. The first scoring volume was placed 5 mm from the edge of the water tank on the central axis. The spheres were 5 mm apart from the next one on the central axis. Thus, the last scoring volume was placed 130 mm from the edge of the water tank on the central axis. The water tank was surrounded by air.

The interactions in the scoring volume ($\varnothing$= 600 µm) and in a 50 µm thick shell surrounding it are simulated with the track structure Geant4-DNA module with the default constructor (option 0). Everywhere else, the interactions are simulated with the condensed history Monte Carlo code using the standard physics modules (g4em-penelope, g4hphy_QGSP_BIC_HP, g4decay, g4ion-binarycascade, g4h-elastic_HP, and g4stopping). Outside the spheres with the 700 µm diameter (i.e. where the interactions are simulated by condensed-history MC) a range cut of 50 µm is used. This speeds up the simulation time since all secondaries with a range of less than 50 µm stop and deposit their energy locally. This way it is guaranteed not to cut off particles, which have the potential to traverse the scoring surface. Moreover, the simulations of the particle interactions inside the 700 µm sphere are detailed, since they are simulated with track structure Monte Carlo simulations. The cut is applied to all types of particles and is internally determined through a conversion between particle energy and range.

II.C. Nanodosimetric Quantities From a Clinical Proton Pencil Beam

To obtain nanodosimetric quantities at different depths of the central axis, the scored charged particle spectra of the clinical proton pencil beam were convoluted with the cluster size distributions. A charged particle equilibrium is assumed in the spheres, i.e. a scored particle spectrum on the surface of the 600 µm scoring sphere is assumed to be valid inside the sphere as well. Two methods were investigated to obtain the cluster size distributions from the simulated charged particle spectra:

Fast Method:

In this method only proton tracks are simulated in the macroscopic volume. The proton energy spectra on the surface of the scoring volumes are convoluted with the corresponding ionization cluster size distributions. The ionization cluster size distributions which consider all ionizations, i.e. ionizations from primary and secondary particles, are used. The obtained cluster size distributions are summed up and then normalized according to equation 1:

$$P_\nu(\Phi_{p^+}) = \frac{\sum_{i=1}^{N_{p^+}} P_\nu(p^+, E_i)}{N_{p^+}} \tag{1}$$

where $\Phi_{p^+} = \{E_1, ..., E_{N_{p^+}}\}$ is the proton spectrum on the surface of the scoring volume, N_{p^+} is the number of protons scored on the surface and E_i is the kinetic energy of the i-th proton.

Slow and Detailed Method:

In this method, proton and electron tracks are simulated in the macroscopic geometry. The proton and electron energy spectra on the surfaces of the scoring volumes are convoluted with the corresponding ionization cluster size distribution. The ionization cluster size distributions, which only consider the ionizations produced by the primary particles, are used. All cluster size distributions are summed and normalized according to equation 2:

$$P_\nu^{\text{prim}}(\Phi_{p^+}, \Phi_{e^-}) = \frac{\sum_{i=1}^{N_{p^+}} P_\nu^{\text{prim}}(p^+, E_i) + \sum_{j=1}^{N_{e^-}} P_\nu^{\text{prim}}(e^-, E_j)}{N_{p^+} + N_{e^-}} \tag{2}$$

where p^+ represents protons, e^- represents electrons and P_ν^{prim} represents the cluster size distributions, which only consider ionizations created by primary particles.

The probability to produce at least two ionizations was then investigated for the two methods, because it is believed to be proportional to DNA double-strand breaks as mentioned above (see I.). For the "fast" method this probability is F_2. To calculate it, the cumulative

probabilities F_2 of all protons are summed up and then averaged:

$$F_2^{\text{fast}} = \frac{\sum_{i=1}^{N_{p^+}} \sum_{\nu=2}^{\infty} P_\nu(p^+, E_i)}{N_{p^+}} \tag{3}$$

For the "slow and detailed" method an interference term has to be added to the F_2 values. The interference term has to account for individual and independent particles which each produce one ionization inside a basic interaction volume, but combined create two or more ionizations:

$$F_2^{\text{slow and detailed}} = \frac{\sum_{i=1}^{N_{p^+}} \sum_{\nu=2}^{\infty} P_\nu^{\text{prim}}(p^+, E_i) + \sum_{j=1}^{N_{e^-}} \sum_{\nu=2}^{\infty} P_\nu^{\text{prim}}(e^-, E_j)}{N_{p^+} + N_{e^-}} + \overline{P}_{\text{interference}} \tag{4}$$

where $\overline{P}_{\text{interference}}$ is the mean interference term. The cases, which contribute to the interference term, are discussed in detail and calculated in the appendix IV.A..

The two types of ionization cluster size distributions are summarized in table 1. The types of Monte Carlo simulations used for the two methods in a macroscopic volume are summarized in table 2.

III. Results

III.A. Database of Ionization Cluster Size Distributions

The ionization cluster size probability for larger clusters is greater when all ionizations are considered compared to when only the ionizations of the primary protons are considered.

In figures 2 and 3, P_1, the probability to produce exactly one ionization, and the cumulative probability F_2 and their energy dependences are shown for protons and electrons. The two different ionization cluster size distributions, "only primaries" and "primaries and secondaries", as defined in section II.A., result also in different probabilities P_1 and different cumulative probabilities F_2.

The probability for protons or electrons to interact with molecules decreases for high velocities. This is reflected in the decrease of F_2 for high energy particles in figures 2 and 3.

For low energies, the cross-sections of elastic scattering increase while the ionization cross-sections decrease which result in a decrease of the F_2 probabilities for particles with low energies.

The behavior of the probability P_1 in the case for protons (figure 2) and in the case for electrons (figure 3) shows in each case two peaks and can be explained in a similar fashion as the behavior of F_2. The probability for high energy charged particles to interact with water molecules decreases with increasing energy which results in decreasing P_1 probabilities. To the left of the peak of P_1 at high energy, i.e. for decreasing energy, the total ionization probability increases. The probabilities for larger cluster sizes increase simultaneously which result in lower probabilities P_1. Once the peak of the total ionization probability is reached (not shown), there is a decrease of the probabilities for large cluster sizes since the cross-sections of elastic scattering increase. This results again in an increase of P_1 for lower energies (first peak). For even lower energies also P_1 decreases since the elastic cross-sections are still increasing.

The shift of the first peak of probability P_1 for the "primaries and secondaries"-method towards lower energies for protons in figure 2, results from the fact that for low energies the influence of the secondary electrons increases substantially. For mid to high energy protons, the influence of the secondary electrons is less important. That is the shape of the peak at high energy is similar for the two different cluster size methods. Nonetheless, the absolute probability of P_1 from the "primaries only"-method is greater than the P_1 probability of the "primaries and secondaries"-method. The reason for this is that the secondary electrons still have influence and increase the probability for larger clusters and hence simultaneously decrease the probability for one ionization.

The total ionization probabilities for TOPAS are larger than for NOREC. This results also in larger F_2 values for TOPAS compared to NOREC as can be seen in figure 3.

III.B. Electron Spectra and Number of Electrons per Proton in the Scoring Spheres

Protons and electrons were recorded up to the 16th sphere located at 80 mm along the z-axis. Farther away on the z-axis, the protons and electrons did not reach any scoring surface. The electron and proton energy spectra scored on the surface of the fifteenth scoring sphere along the z-axis at 80 mm are shown in figure 4. The spectra are shifted towards lower energies

for deeper located spheres. Also the relative number of electrons to protons increases (see table 3 for specific numbers).

From the charged particle spectra along the central axis, the mean electron and proton energies were determined. From the electron energy spectra the range spectra was obtained. The energy-range conversion values were acquired from Wilson et al.[23]. The median electron range in the first 16 spheres along the z-axis was 6.8 nm for each sphere. Additionally, the mean numbers of scored electrons per proton on the surfaces of the spheres along the z-axis were determined and are listed in table 3.

III.C. F_2 Obtained with the "Fast" and with the "Slow and Detailed" Method for a Clinical Proton Pencil Beam

The cumulative probability F_2 at 5 mm as a function of the number of simulated primary protons is shown in figure 5. For the "slow and detailed" method, the cumulative probabilities obtained with TOPAS (triangle pointing upwards) and with NOREC (triangle pointing downwards) are shown.

The "fast" method converges quickly to a constant value, whereas the "slow and detailed" method requires a larger number of histories to be simulated in order to converge. Moreover, the "fast" method produces a cumulative F_2, which lies between the cumulative F_2's of the two approaches of the "slow and detailed" method. The "slow and detailed" method where the electron cluster size distributions were calculated with NOREC produced the lowest value for the cumulative F_2 at the first scorer. The second approach of the "slow and detailed" method, where the electron cluster size distributions were calculated with TOPAS, results in the largest values for the cumulative F_2's at the location of the first scorer.

The mean probabilities F_2 obtained with the "fast" and the "slow and detailed" methods along the central axis z are shown in figure 6. The F_2 obtained from the "fast" method, where the spectrum of the protons was convoluted with the ionization cluster size distributions of the primary protons and secondary electrons, are represented with star symbols. The mean probabilities F_2 obtained from the "slow and detailed" method are represented by triangles (pointing upwards when the electron cluster sizes were simulated with TOPAS and pointing downwards when simulated with NOREC). As can be seen, the "fast" method yields mean cumulative probabilities F_2 which are always between the probabilities obtained

by the "slow and detailed" method, where the electrons were simulated with NOREC and where the electrons were simulated with TOPAS.

The "fast" method is expected to yield the same results for F_2 as the "slow and detailed" TOPAS method but instead large differences are observed. A possible explanation for the observed differences can be that the contributions of electrons from the same track further away and from adjacent proton tracks have a non-negligible effect on the ionization distributions. The percentages of electrons neglected in the "fast" method were estimated and are listed in table 3. A detailed calculation of the estimation of the neglected number of electrons is given in the appendix IV.B..

IV. Discussion

An open question, when obtaining nanodosimetric quantities for proton treatment planning, is, whether fast macro Monte Carlo codes, combined with track structure simulations for the secondary particles, are accurate enough for the determinations of the cluster size distributions as suggested by Ramos-Méndez et al.[14]. A limitation of this method is the potential contamination of proton tracks with electrons from adjacent protons. By comparing "proton only" simulations with detailed simulations of all protons and electrons using TOPAS, it was observed that the "proton only approach" yields on average a 48% error in the nanodosimetric quantity F_2 compared to the "slow and detailed" method. It was shown that this uncertainty is related to the omission of electrons which were created further away. Therefore, the calculation of nanodosimetric quantities with a "proton only approach" must be used with care.

Another important finding is the impact of the different Monte Carlo codes on the cluster size distributions of electrons. It was found, that on average the F_2 probabilities, where the electron cluster sizes were obtained with NOREC, were 55% smaller than the F_2 probabilities where all cluster sizes were obtained with TOPAS. One reason for this deviation is the use of different cross-sections and models for electron interactions. The total ionization probability in a basic interaction volume over all energies is 30% lower for electrons simulated with NOREC compared to the total ionization probability obtained with TOPAS. This result is in agreement with the findings of Incerti et al.[16] who showed that on average more energy is required to produce an ion in liquid water with NOREC compared to Geant4-DNA (con-

structor options 2,4, and 6) (see figure 5 in[16]). Hence, more research is needed for obtaining precise electron interaction cross-sections.

It was observed, that the cumulative cluster size probabilities for clusters greater or equal to one produced by an electron is always greater in the simulations with TOPAS than in the simulations with NOREC (e.g. see figure 3). As a result F_2 from NOREC is always smaller than the TOPAS F_2 as shown in figure 3. Similar results were obtained before by Lazarakis et al. where Geant4-DNA produced systematically larger ionization clusters for electrons below 300 eV than the Monte Carlo code PTra.[18]

In figure 5, the "fast" method converges with only a few numbers of simulated particles, whereas the "slow and detailed" method requires a much larger number of particles to be simulated in order for F_2 to converge. An explanation for this rapid convergence of the "fast" method is that the scored energy spectra of the protons never exceed two orders of magnitude (see figure 4). Additionally, most protons have high energies where their cumulative probability F_2 is not changing strongly (see the energy dependence of F_2 for protons in figure 2). In contrast the energy spectra of the electrons span over more than five orders of magnitudes and more important these electron spectra are for lower energies where they span over the whole range of changing F_2 values (see the energy dependence of F_2 for electrons in figure 3). Hence, more particles are required to adequately cover the whole energy range and their corresponding F_2 values in case of the electrons. Accordingly the "slow and detailed" method requires more number of particles as well since the F_2 values of the electrons are taken into consideration separately.

It has been shown that the "fast" method, where only protons are simulated, is essentially inadequate to describe cluster size distributions and hence F_2 probabilities. However, it has also been shown that the F_2 probabilities of the "slow and precise" method, where the electron cluster sizes were simulated with NOREC, deviate even more from the F_2 probabilities of the slow and precise method, where the electrons were simulated with TOPAS, than the F_2 probabilities from the "fast" method. Therefore, as long as the electron Monte Carlo codes cross-sections and models are not improved, it is feasible to use the "fast" proton method. It must be noted however, that the uncertainty is of the order of 100%. Additionally, an alternative construction option (option 4) with improved cross-sections and with an alternative elastic scattering model is available in Geant4-DNA.[24] This results in strongly enhanced excitations relative to ionizations, more accurate ionization cross-sections near the

binding energies and a less accurate elastic scattering model at low energies.[25] Especially, for electrons with an energy below 100 eV, significantly lower ionization cross-sections are obtained with this alternative option.[26] It is to be assumed that with these alternative cross-sections the difference between NOREC and TOPAS would be reduced. Nevertheless, the mean F_2 values obtained with option 4 will very likely still be larger than the F_2 values from NOREC since the mean energy required to produce an ionization is still consistently larger in NOREC as can be seen in figure 5 in the publication of Incerti et al.[16]. If the result of NOREC or option 4 of the Geant4-DNA Monte Carlo code are closer to reality is still undetermined. Hence, further investigation of the impact of these cross-sections on the cumulative probability F_2 in a macroscopic volume could be interesting.

In physics the gold standard to verify results is to compare them with measurements. Unfortunately, it is not yet possible to measure cluster size distributions in biological tissue. A detector, which would be able to determine the cluster sizes in a phantom, representing a patient, needs to fulfil additional requirements compared to a nanodosimeter which determines a cluster size in one volume. Such a detector needs to be able to measure single ionizations over a large area with high resolution. One possible nanodosimetric detector which could be able to measure such cluster sizes along the primary particle track is the track imaging detector currently developed at University of Zurich and firstly suggested by Bashkirov et al.[27 2 28 29 30]

Appendix

IV.A. Interference Contributions to F_2

If in the "slow and detailed" method only the cumulative probabilities F_2 of the individual and independent particles are considered, then the probabilities to produce two or more ionizations is underestimated. The cases when several independent particles which ionize once but combine to clusters of two or more ionizations together have to be taken into account. These interference probabilities depend on the mean number of electrons per proton. Since we are interested in the probability to have more than two ionizations in a basic interaction volume we have to account for these cases in the "slow and detailed" method. The mean contributions per proton can be calculated as following:
The mean interference probability assuming there are n_{ep} electrons per proton is given by equation 5:

$$\overline{P}_{\text{interference}}(\geq \text{two ionizations} \mid n_{ep} \text{ electrons}) = n_{ep} \times \overline{p_1^{p+}} \times \overline{p_1^{e-}} + \sum_{k=2}^{n_{ep}} \binom{n_{ep}}{k} (\overline{p_1^{e-}})^k \qquad (5)$$

where $n_{ep} \in \mathbb{N}$, $\overline{p_1^{p+}}$ and $\overline{p_1^{e-}}$ are the mean probabilities of the protons and electrons to produce one ionization, respectively.

The mean number of electrons per proton $\overline{n_{ep}}$ is usually not a natural number (i.e. $\overline{n_{ep}} \notin \mathbb{N}$). To calculate the mean interference probability in each sphere, the interference probabilities were calculated for the two closest natural numbers and averaged accordingly.

IV.B. Estimating the Number of Electrons Neglected by the "Fast" Method

The difference of the "fast" method and the "slow and detailed" method when the same Monte Carlo code is used presumably comes from excessive number of electrons in the "slow and detailed" method which ionize outside of the basic interaction volume where they were created. The "fast" method only takes the electrons into consideration which are generated and ionize inside the basic interaction volumes.

For verification purposes, the "fast" method should be reproducible by the "slow and detailed" method when using less electrons. For that purpose the number of electrons per proton in the scoring surface which would come from single basic interaction volumes has to be estimated. For this estimation two layers of basic interaction volumes which adjoin the scoring surface are considered since the velocity vector of these electrons is assumed to be isotropic (see figure 7).

To estimate the number of electrons of the "fast" method which would intersect the scoring surface two layers of basic interaction volumes which adjoin the scoring surface are considered since the velocity vector of these electrons is assumed to be isotropic (see figure 7).

The number of electrons which are produced by a proton track is proportional to the number of basic interaction volumes traversed by the proton. Thus the number of scored electrons is proportional to the mean chord length of a parallel proton beam through a spherical shell. The mean chord length $\overline{L}$ of a spherical shell is:

$$\overline{L} = \frac{\frac{4}{3} \times (R^3 - r^3)}{R^2} \tag{6}$$

where R is the outer and r the inner radius of the spherical shell.[31]
By traversing a spherical shell with an outer radius $R = 300\,\mu\text{m} + 2.5\,\text{nm}$ and an inner radius $r = 300\,\mu\text{m} - 2.5\,\text{nm}$, the mean chord length $\overline{L}$ equals 20 nm, hence a proton intersects on average 8 basic interaction volumes. The mean number of electrons produced by a proton in the basic interaction volume was simulated for the mean proton energies of the scoring surfaces. The resulted number of electrons coming from the layers of basic interaction volumes adjoining the scoring spheres are listed above in table 3.

References

[1] A. M. Kellerer, Fundamentals of Dosimetry and Microdosimetry and the Relative Biological Effectiveness of Ionizing Radiations, pages 123–140, Springer US, Boston, MA, 1985.

[2] R. W. Schulte, Nanodosimetry: Principle and Current Status, AIP Conference Proceedings **1345**, 249–261 (2011).

[3] B. Grosswendt, Recent advances of nanodosimetry, Radiation Protection Dosimetry **110**, 789–799 (2004).

[4] B. Grosswendt, Nanodosimetry, from radiation physics to radiation biology, Radiation Protection Dosimetry **115**, 1–9 (2005).

[5] B. Grosswendt, S. Pszona, and A. Bantsar, New descriptors of radiation quality based on nanodosimetry, a first approach, Radiation Protection Dosimetry **126**, 432–444 (2007).

[6] H. Rabus and H. Nettelbeck, Nanodosimetry: Bridging the gap to radiation biophysics, Radiation Measurements **46**, 1522 – 1528 (2011), Proceedings of the 16th Solid State Dosimetry Conference , September 19-24 , Sydney , Australia.

[7] H. Palmans, H. Rabus, A. L. Belchior, M. U. Bug, S. Galer, U. Giesen, G. Gonon, G. Gruel, G. Hilgers, D. Moro, H. Nettelbeck, M. Pinto, A. Pola, S. Pszona, G. Schettino, P. H. G. Sharpe, P. Teles, C. Villagrasa, and J. J. Wilkens, Future development of biologically relevant dosimetry, The British Journal of Radiology **88**, 20140392 (2015), PMID: 25257709.

[8] A. Schipler and G. Iliakis, DNA double-strandbreak complexity levels and their possible contributions to the probability for error-prone processing and repair pathway choice, Nucleic Acids Research **41**, 7589–7605 (2013).

[9] N. T. Henthorn, J. W. Warmenhoven, M. Sotiropoulos, R. I. Mackay, K. J. Kirkby, and M. J. Merchant, Nanodosimetric Simulation of Direct Ion-Induced DNA Damage Using Different Chromatin Geometry Models, Radiation Research **188**, 770 – 783 (2017).

[10] H. Nikjoo, D. Emfietzoglou, T. Liamsuwan, R. Taleei, D. Liljequist, and S. Uehara, Radiation track, DNA damage and response—a review, Reports on Progress in Physics **79**, 116601 (2016).

[11] D. Brenner and J. Ward, Constraints on Energy Deposition and Target Size of Multiply Damaged Sites Associated with DNA Double-strand Breaks, International Journal of Radiation Biology **61**, 737–748 (1992).

[12] M. Casiraghi and R. W. Schulte, Nanodosimetry-Based Plan Optimization for Particle Therapy, Computational and Mathematical Methods in Medicine **2015**, 1–13 (2015).

[13] F. Alexander, C. Villagrasa, H. Rabus, and J. J. Wilkens, Local weighting of nanometric track structure properties in macroscopic voxel geometries for particle beam treatment planning, Physics in Medicine and Biology **60**, 9145–9156 (2015).

[14] J. Ramos-Méndez, L. N. Burigo, R. Schulte, C. Chuang, and B. Faddegon, Fast calculation of nanodosimetric quantities in treatment planning of proton and ion therapy, Physics in Medicine & Biology **63**, 235015 (2018).

[15] S. Incerti, G. Baldacchino, M. Bernal, R. Capra, C. Champion, Z. Francis, P. Guèye, A. Mantero, B. Mascialino, P. Moretto, P. Nieminen, C. Villagrasa, and C. Zacharatou, THE GEANT4-DNA PROJECT, International Journal of Modeling, Simulation, and Scientific Computing **01**, 157–178 (2010).

[16] S. Incerti, I. Kyriakou, M. A. Bernal, M. C. Bordage, Z. Francis, S. Guatelli, V. Ivanchenko, M. Karamitros, N. Lampe, S. B. Lee, S. Meylan, C. H. Min, W. G. Shin, P. Nieminen, D. Sakata, N. Tang, C. Villagrasa, H. N. Tran, and J. M. C. Brown, Geant4-DNA example applications for track structure simulations in liquid water: A report from the Geant4-DNA Project, Medical Physics **45**, e722–e739 (2018).

[17] M. Bernal et al., Track structure modeling in liquid water: A review of the Geant4-DNA very low energy extension of the Geant4 Monte Carlo simulation toolkit, Physica Medica **31**, 861 – 874 (2015).

[18] P. Lazarakis, M. U. Bug, E. Gargioni, S. Guatelli, H. Rabus, and A. B. Rosenfeld, Comparison of nanodosimetric parameters of track structure calculated by the Monte Carlo codes Geant4-DNA and PTra, Physics in Medicine & Biology **57**, 1231 (2012).

[19] P. Lazarakis, S. Incerti, V. Ivanchenko, I. Kyriakou, D. Emfietzoglou, S. Corde, A. B. Rosenfeld, M. Lerch, M. Tehei, and S. Guatelli, Investigation of track structure and condensed history physics models for applications in radiation dosimetry on a micro and nano scale in Geant4, Biomedical Physics & Engineering Express **4**, 024001 (2018).

[20] M. Bug, H. Rabus, and A. Rosenfeld, Electron emission from amorphous solid water after proton impact: Benchmarking PTra and Geant4 track structure Monte Carlo simulations, Radiation Physics and Chemistry **81**, 1804 – 1812 (2012).

[21] M. Dingfelder, R. H. Ritchie, J. E. Turner, W. Friedland, H. G. Paretzke, and R. N. Hamm, Comparisons of Calculations with PARTRAC and NOREC: Transport of Electrons in Liquid Water, Radiation Research **169**, 169 – 169 – 11 (2008).

[22] V. A. Semenenko, J. E. Turner, and T. B. Borak, NOREC, a Monte Carlo code for simulating electron tracks in liquid water, Radiation and Environmental Biophysics **42**, 213–217 (2003).

[23] W. E. Wilson, J. H. Miller, D. J. Lynch, R. R. Lewis, and M. Batdorf, Analysis of Low-Energy Electron Track Structure in Liquid Water, Radiation Research **161**, 591–596 (2004).

[24] I. Kyriakou, S. Incerti, and Z. Francis, Technical Note: Improvements in geant4 energy-loss model and the effect on low-energy electron transport in liquid water, Medical Physics **42**, 3870–3876 (2015).

[25] I. Kyriakou, D. Emfietzoglou, V. Ivanchenko, M. C. Bordage, S. Guatelli, P. Lazarakis, H. N. Tran, and S. Incerti, Microdosimetry of electrons in liquid water using the low-energy models of Geant4, Journal of Applied Physics **122**, 024303 (2017).

[26] I. Kyriakou, M. efl, V. Nourry, and S. Incerti, The impact of new Geant4-DNA cross section models on electron track structure simulations in liquid water, Journal of Applied Physics **119**, 194902 (2016).

[27] V. A. Bashkirov, R. F. Hurley, and R. W. Schulte, A novel detector for 2D ion detection in low-pressure gas and its applications, in *2009 IEEE Nuclear Science Symposium Conference Record (NSS/MIC)*, pages 694–698, 2009.

[28] M. Casiraghi, V. Bashkirov, F. Hurley, and R. Schulte, A novel approach to study radiation track structure with nanometer-equivalent resolution, The European Physical Journal D **68**, 111 (2014).

[29] M. Casiraghi, V. A. Bashkirov, R. F. Hurley, and R. W. Schulte, Characterisation of a track structure imaging detector, Radiation Protection Dosimetry **166**, 223–227 (2015).

[30] F. Vasi, M. Casiraghi, V. Bashkirov, U. Giesen, and R. Schulte, Development of a single ion detector for radiation track structure studies, Journal of Instrumentation **11**, C09021–C09021 (2016).

[31] A. M. Kellerer, Considerations on the Random Traversal of Convex Bodies and Solutions for General Cylinders, Radiation Research **47**, 359–376 (1971).

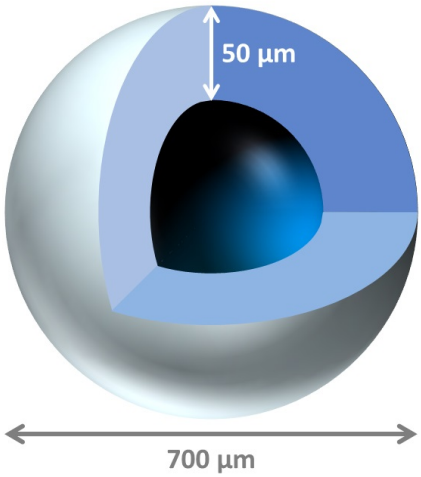

Figure 1: The spherical scoring volume, here the inner, dark blue sphere, has a diameter of 600 µm and is surrounded by a 50 µm thick shell. In these 700 µm spheres track structure Monte Carlo simulations are performed to assure that the scored spectra on the surfaces of the 600 µm spheres are accurate.

Table 1: Atlas of Ionization Cluster Size Distributions in the Basic Interaction Volume

Ionization Cluster Size Distribution Type	**Type of Monte Carlo code**	**Material inside sphere**	**Material surrounding the sphere**	**Ionizations considered from**
Only primaries	track structure	liquid water	vacuum	primary protons or primary electrons
Primaries and secondaries	track structure	liquid water	liquid water	all charged particles

Table 2: Clinical Proton Pencil Beam

Method	**Type of MC code outside 700 µm sphere**	**Type of Monte Carlo code inside 700 µm sphere**	**Charged particle spectra**	**Convolution of charged particle spectra with ICSD of type**
Fast	Macro	track structure	only protons	primaries and secondaries
Slow and Detailed	Macro	track structure	all charged particles	only primaries

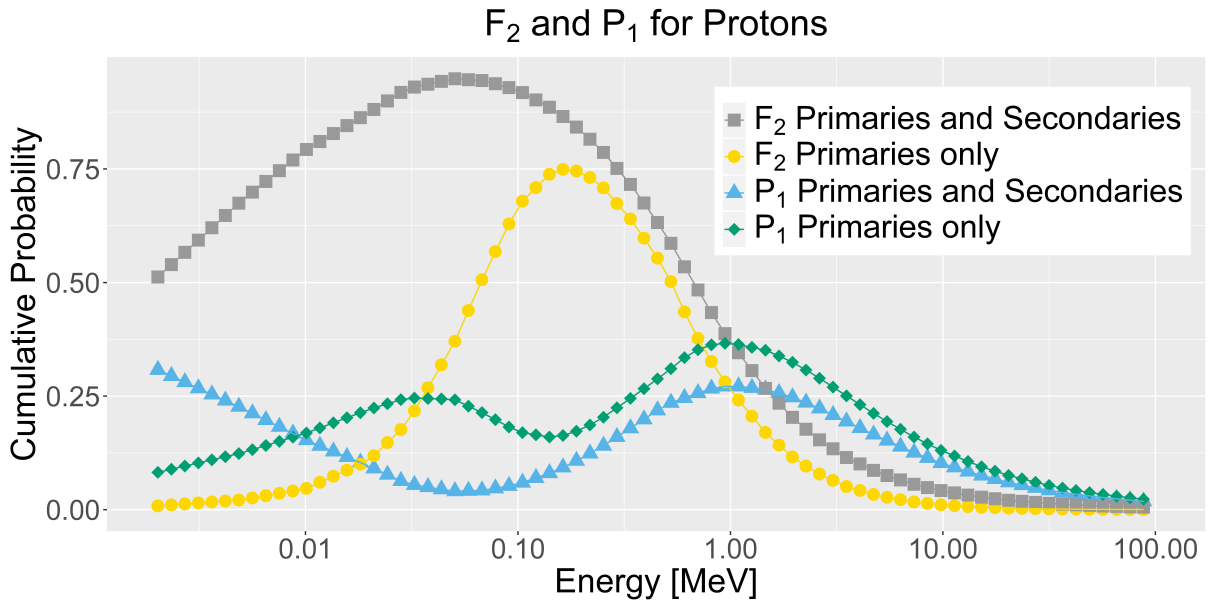

Figure 2: The energy dependence of F_2 in the basic interaction volume with a diameter of 2.48 nm corresponding to a volume of 8 nm^3 for protons. "Only primaries" refers to the ionization cluster size distributions where the contributions of the secondary particles were excluded as defined in II.A..

Table 3: Location of the scoring sphere on the central axis, mean energy of the scored electrons, mean range of the scored electrons, mean energies of the scored protons, the mean number of electrons per proton in the surfaces of the scoring spheres, and the mean number of electrons per proton in the scoring spheres originated in two layers of basic interaction volumes (BIVs) [for details see III.C., the appendix IV.B. and figure 7].

z[cm]	$E^{e^-}_{mean}$[keV]	$R^{e^-}_{mean}$[nm]	$E^{p^+}_{mean}$[MeV]	e^-/p^+	e^-/p^+ in two layer of BIVs
0.5	21.7	24 867	95.5	0.62	0.24
1.0	21.1	23 230	91.6	0.61	0.25
1.5	20.1	20 728	87.7	0.62	0.25
2.0	19.5	20 608	83.7	0.65	0.27
2.5	18.6	18 061	79.5	0.68	0.28
3.0	15.9	13 654	75.1	0.69	0.30
3.5	15.0	12 199	70.5	0.73	0.32
4.0	14.5	13 233	65.7	0.78	0.35
4.5	12.4	9728	60.6	0.82	0.38
5.0	11.1	7191	55.1	0.85	0.40
5.5	9.5	5885	49.2	0.93	0.43
6.0	7.9	4079	42.6	0.99	0.49
6.5	6.2	3938	35.1	1.13	0.58
7.0	4.1	2191	25.9	1.38	0.74
7.5	1.3	967	12.8	2.40	1.32
8.0	0.3	39	5.4	3.72	2.82

Last edited *Date* :

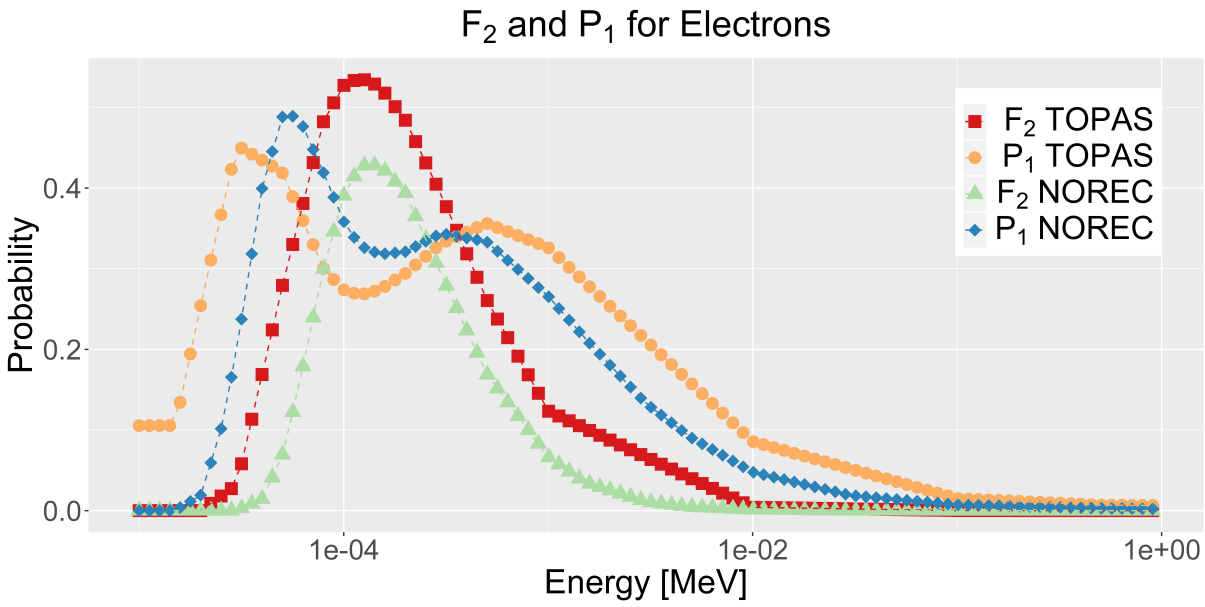

Figure 3: F_2 and P_1 for electrons calculated from the "only primary" ionization cluster size distributions in the basic interaction volume with a diameter of 2.48 nm (see II.A. for more information). The cluster size distributions were simulated by the two Monte Carlo codes TOPAS and NOREC.

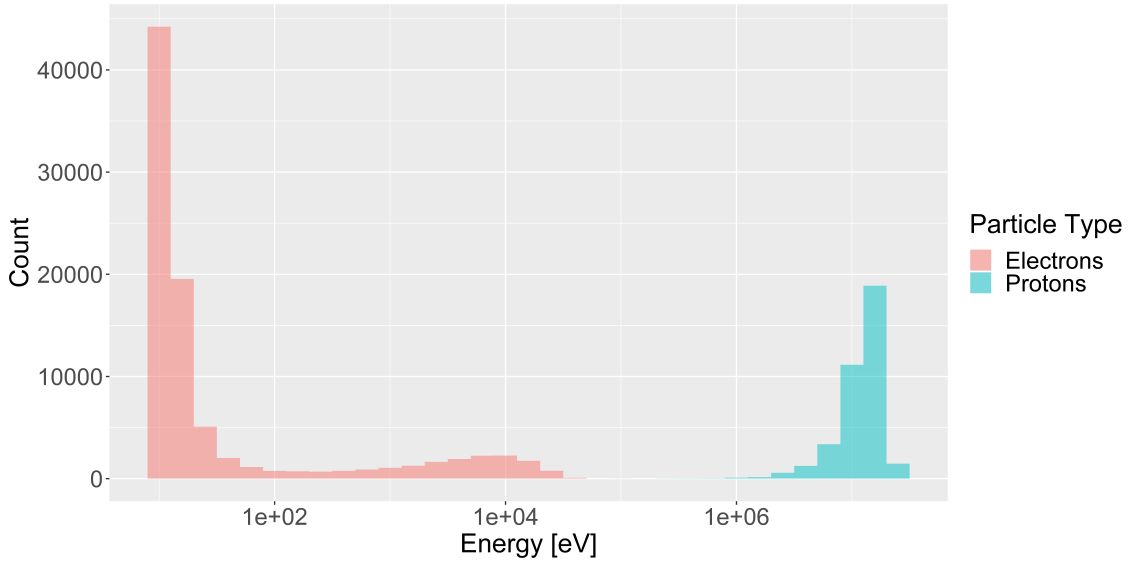

Figure 4: Electron and proton spectra at a depth of 75 mm (sphere number 15).

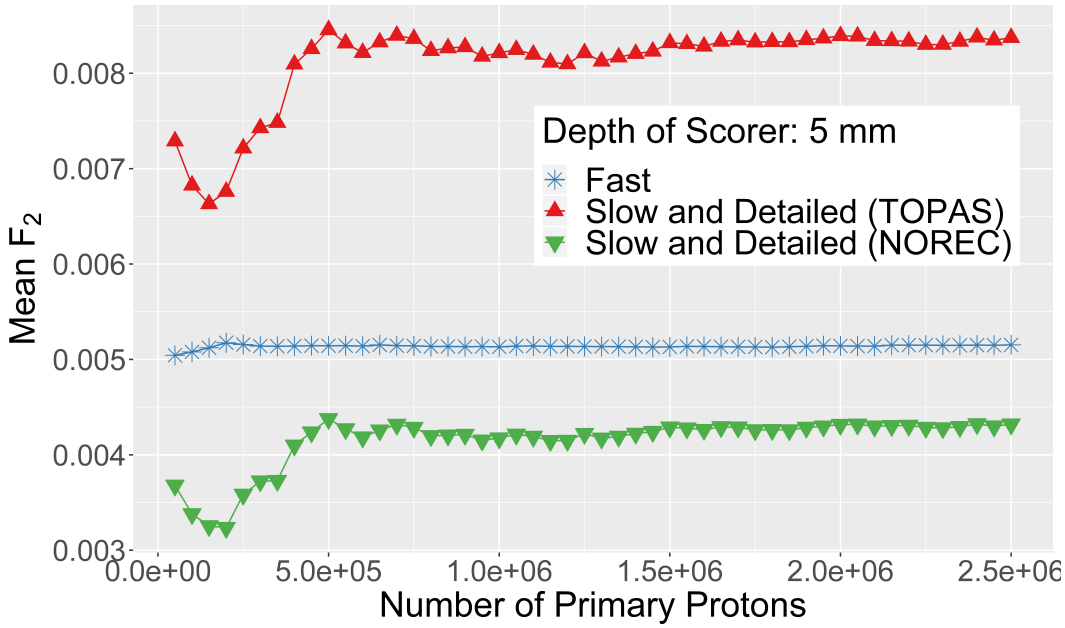

Figure 5: F_2 for an increasing number of simulated histories at the first scorer on the central axis. The star symbols represent the values from the "fast" method, where the proton spectrum was convoluted with the cumulative cluster size distributions F_2 which include ionizations from electrons. The triangles represent the mean cumulative probability F_2 of the "slow and detailed" method, where the interference term was not added. The triangles pointing downwards represent the mean F_2 values, where the electron ICSD were simulated with NOREC. The triangle pointing upwards represent the values, where the electron ICSD were obtained with TOPAS.

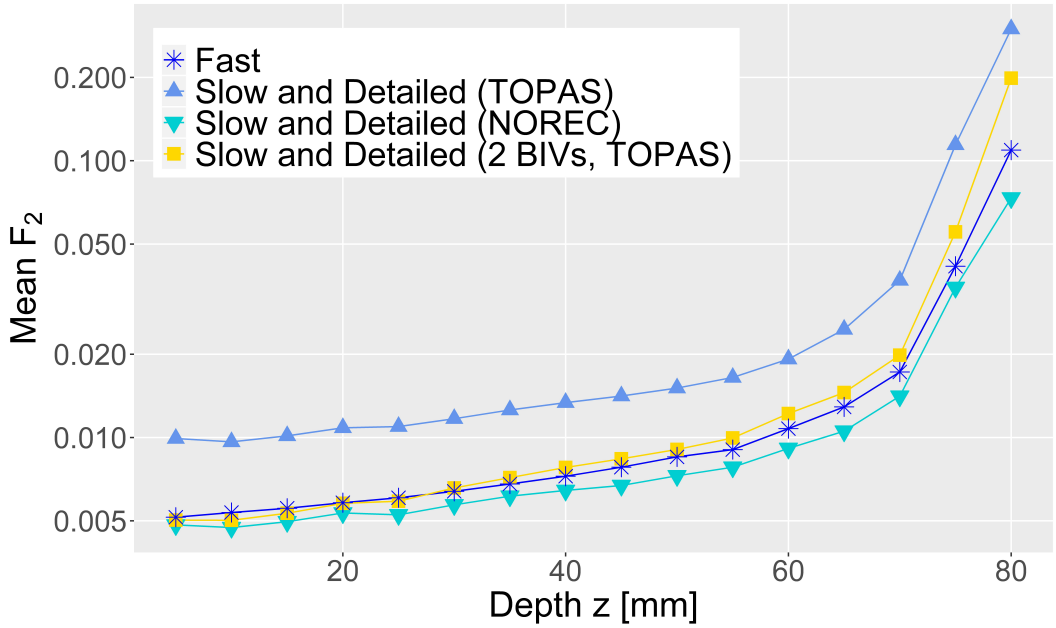

Figure 6: Mean F_2 values along the central axis z are shown. The star symbols represent the values from the "fast" method. The triangles pointing upwards represent the values of F_2 obtained from the "slow and detailed" method, where the electrons were simulated with TOPAS. The triangles pointing downwards represent the values of F_2 obtained from the "slow and detailed" method, where the electrons were simulated with NOREC. The squares represent the values of the mean F_2 values, which were acquired in the same way as in the "slow and detailed" method but with a reduced number of electrons because it is assumed that the "fast" method underestimates the number of electrons. For more information see the text and the appendix.

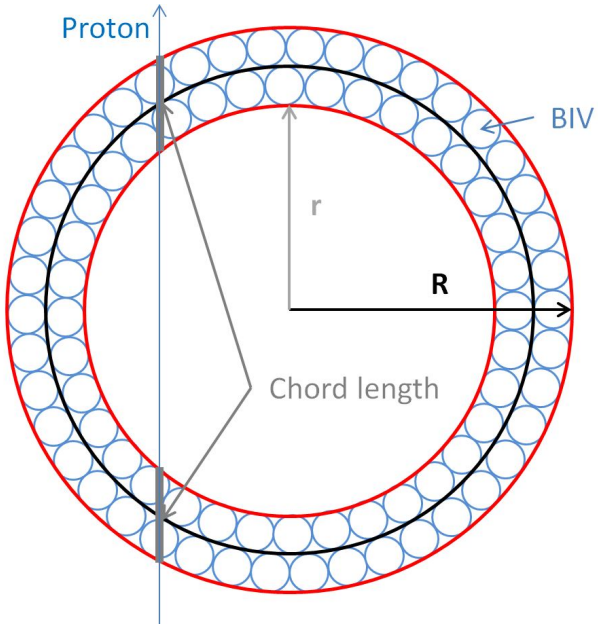

Figure 7: A scoring sphere with layers of basic interaction volumes adjoining the scoring surface.

- The spherical scoring volume, here the inner, dark blue sphere, has a diameter of 600 µm and is surrounded by a 50 µm thick shell. In these 700 µm spheres track structure Monte Carlo simulations are performed to assure that the scored spectra on the surfaces of the 600 µm spheres are accurate.

- The energy dependence of F_2 in the basic interaction volume with a diameter of 2.48 nm corresponding to a volume of 8 nm^3 for protons. "Only primaries" refers to the ionization cluster size distributions where the contributions of the secondary particles were excluded as defined in II.A..

- F_2 and P_1 for electrons calculated from the "only primary" ionization cluster size distributions in the basic interaction volume with a diameter of 2.48 nm (see II.A. for more information). The cluster size distributions were simulated by the two Monte Carlo codes TOPAS and NOREC.

- Electron and proton spectra at a depth of 75 mm (sphere number 15).

- F_2 for an increasing number of simulated histories at the first scorer on the central axis. The star symbols represent the values from the "fast" method, where the proton spectrum was convoluted with the cumulative cluster size distributions F_2 which include ionizations from electrons. The triangles represent the mean cumulative probability F_2 of the "slow and detailed" method, where the interference term was not added. The triangles pointing downwards represent the mean F_2 values, where the electron ICSD were simulated with NOREC. The triangle pointing upwards represent the values, where the electron ICSD were obtained with TOPAS.

- Mean F_2 values along the central axis z are shown. The star symbols represent the values from the "fast" method. The triangles pointing upwards represent the values of F_2 obtained from the "slow and detailed" method, where the electrons were simulated with TOPAS. The triangles pointing downwards represent the values of F_2 obtained from the "slow and detailed" method, where the electrons were simulated with NOREC. The squares represent the values of the mean F_2 values, which were acquired in the same way as in the "slow and detailed" method but with a reduced number of electrons because it is assumed that the "fast" method underestimates the number of electrons. For more information see the text and the appendix.

589 • A scoring sphere with layers of basic interaction volumes adjoining the scoring surface.

590 "The authors have no conflicts to disclose."